

Bilayer graphene nanoribbon nanoelectromechanical system device: A computational study

Kai-Tak Lam, Chengkuo Lee, and Gengchiao Liang^{a)}

Department of Electrical and Computer Engineering, National University of Singapore, Singapore 117576, Singapore

(Received 20 July 2009; accepted 15 September 2009; published online 6 October 2009)

A bilayer graphene nanoribbon nanoelectromechanical device is investigated via first-principle simulations. The output characteristics as a function of interlayer distance are calculated, with the proposed device acting as a displacement and a force sensor. The operating mechanism of a bistable switch based on this device structure is also explored, and in the present floating gate design, a switching gate bias of 5.6 V is required, resulting in an ON-OFF current ratio of 3 orders at a device bias of 20 mV. This minuscule bistable device could potentially be implemented in future semiconductor memory devices and radio frequency communication circuitry. © 2009 American Institute of Physics. [doi:10.1063/1.3243695]

Recently, considerable development on nanoelectromechanical system (NEMS) technology has shown great potential as an innovative approach to implement electrical and mechanical functionalities at the nanometer scale. Promising characteristics of NEMS devices, for example, high mechanical resonance frequency and low power requirement for device operations, have enabled attractive applications such as ultrafast switches,^{1–4} highly sensitive mass detectors,⁵ and high-speed low-power random access memory cells.^{6–8} To develop high-performance NEMS, material properties, i.e., high spring constants, small mass, and high electron mobility, play important roles on improving device sensitivity, switching speeds, operating power requirements, and other characteristics.

Additionally, recent investigations of carbon as an electronic material have been increased due to the availability of thermodynamically stable monolayer planar carbon,^{9–11} better known as graphene. Graphene provides unique electronic properties for device applications, i.e., high carrier mobility¹² and the ability to alter the energy bandgap (E_g) by changing its geometry.¹³ While two-dimensional graphene is a semimetal, its one-dimensional derivative graphene nanoribbon (GNR) is a semiconductor, whose E_g is closely related to its width due to the quantum confinement introduced by the edges. In addition to the monolayer graphene, its bilayer counterpart has also generated much interest, since theoretical studies^{14–16} and experimental observations^{17,18} have shown that a perpendicularly applied electric field can induce an E_g in the otherwise semimetallic material. Nevertheless, for bilayer graphene, a relatively large electric field is required to produce a significant E_g (5 V/nm for an E_g of 0.27 eV). In contrast, bilayer GNRs (BGNRs) exhibit an intrinsic E_g , which is sensitive to both the ribbon width and the interlayer distance (D) between the monolayers.¹⁹

Based on this unique property, in this letter, we propose a BGNR NEMS device for sensor and switch applications [cf. Figs 1(a) and 1(b)]. The operating principle of the proposed device is introduced and it is observed that the current-voltage characteristics of this device can be modulated by D

of BGNRs due to the different bandgap related to the variation in D . Next, density functional theory models, coupled with nonequilibrium Green's function approach, implemented in ATOMISTIX TOOLKIT 2008.02 (Ref. 20) were then employed to investigate the device physics and to evaluate the device performance at different D . Furthermore, the pressure perpendicular to the plane of the device was extracted for different D and an analytical study was then carried out on a possible NEMS switch structure to demonstrate the proposed operating mechanism.

The NEMS device studied is a Schottky contact transistor consisting of an active region of armchair-edged BGNR (A-BGNR), contacted with zigzag-edged BGNR, as shown in Figs. 1(c) and 1(d). The E_g dependency on D of a 1.1-nm-wide A-BGNR with $E_g=0.7$ eV at the relaxed $D=3.2$ Å was calculated. As shown in Fig. 2(a), it was observed that

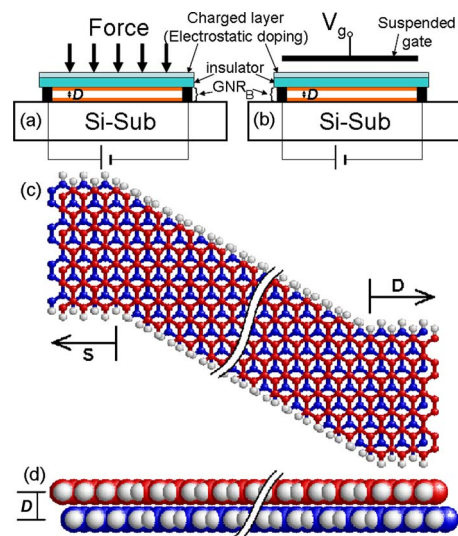


FIG. 1. (Color online) A schematic of the BGNR device implemented as (a) a force sensor and (b) a nanoelectromechanical switch. An atomic representation of the BGNR nanoelectromechanical device is shown in (c). The edges of the bilayer are passivated with hydrogen (white) atoms. The source (s) and drain (d) of the device are zigzag edged BGNR, while the channel is armchair edged BGNR and is bent at 30° with respect to the contacts. (d) The side view of the device is shown where the covalent radii of the atoms are represented.

^{a)} Author to whom correspondence should be addressed. Electronic mail: elelg@nus.edu.sg.

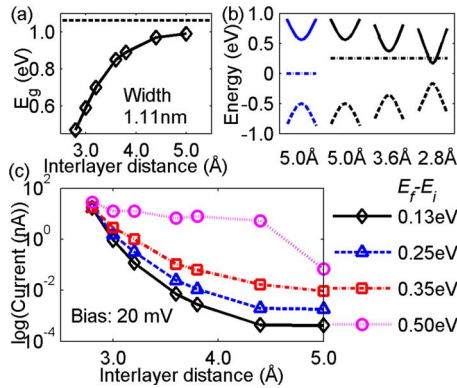


FIG. 2. (Color online) (a) The energy bandgap (E_g) dependency on the interlayer distance (D) with the dashed line representing the E_g of the monolayer counterpart. The operating principle of the device is summarized in (b). At the given electrostatic doping (e.g., 0.25 eV), as D decreases, the E_g decreases, and the conduction band (E_c , solid line) moves closer to the Fermi energy (E_F , dotted-dashed line). As the E_c crosses E_F , the device is completely turned on and a large current is obtained. (c) The current-voltage characteristics of the device at different electrostatic doping conditions ($E_F - E_i$). The device is in ON-state when D is small, and in OFF-state at large D .

the E_g increased monotonically as D increased from 2.8 to 5.0 Å and approaches that of the monolayer (1.06 eV, dashed line). Based on this relationship, a NEMS device following the operating principle visualized in Fig. 2(b) was considered. The conduction band (solid line, E_c) and the valence band (dashed line, E_v) at different D are shown, with the dashed-dotted line representing the Fermi level E_F . The band diagram at the left represents the E_c and E_v of the intrinsic A-BG NR with the width of 1.1 nm and $D=5.0$ Å. An electrostatic doping, e.g., $E_F - E_i = 0.25$ eV, where E_i represents the intrinsic Fermi energy, can be applied on the device, which shifts the E_F closer to the E_c . This E_F position is then fixed for the rest of the plots. As D decreases, the E_g decreases and the E_c moves closer to E_F , and eventually crosses the E_F at $D=2.8$ Å. As a result, the conductivity around the E_F of this A-BG NR should increase as D decreases when the E_F is aligned inside the conduction band.

Based on this principle and possible device structures as shown in Figs. 1(a) and 1(b), the current-voltage characteristics of the NEMS device were simulated under a bias of 20 mV across the active region at various electrostatic doping, ranging from 0.13 to 0.50 eV as a function of D in Fig. 2(c). First, a reduction in the current as D increase was observed, and the OFF-state current (I_{OFF}), where $D=5.0$ Å, was found to increase with the doping level, while the ON-state current (I_{ON}), where $D=2.8$ Å stayed relatively similar as the doping level varied. The observed difference is due to the positioning of E_F . In the former case where $D=5.0$ Å, the E_F was aligned much lower than E_c and it moved away from E_c with decreasing doping level. As a result, the I_{OFF} , which was predominated by tunneling currents, decreased as E_F was far away from E_c . This also indicates that I_{OFF} can be further suppressed by increasing the channel length. On the other hand, for the latter case with $D=2.8$ Å, E_F was close to or even above E_F under low doping level, and hence, the I_{ON} , which was mainly due to electrons transport above the conduction band, was relatively stable and its variation was not obvious in the logarithmic scale. This results in the increase in the I_{ON} to I_{OFF} ratio ($I_{\text{ON}}/I_{\text{OFF}}$) with decreasing electro-

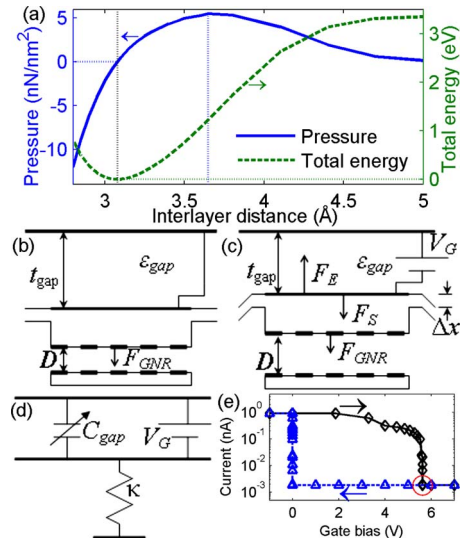


FIG. 3. (Color online) (a) The pressure (upward positive) perpendicular to the plane of the device and the total energy (normalized to the minimum value) are plotted against D . The minimum pressure required to switch the device is 5.51 nN/nm². Schematic of the BG NR NEMS switch at (b) initial state and when (c) a gate bias (V_G) is applied. The dashed lines represent the BG NR and the mobile electrode is attached to an oxide layer grown above the BG NR. (d) A simple model used for the analysis of the parallel plate actuator floating gate. (e) The current characteristics of the NEMS switch as the V_G varies. The solid line shows the current changes as the forward V_G is applied and the dashed line shows the V_G in reverse. The circle indicates the threshold gate bias (V_{th}) where the device switches from ON-state to OFF-state.

static doping. Furthermore, at a high electrostatic doping of 0.5 eV, the currents stayed relatively the same as D increased from 2.8 to 4.4 Å and dropped sharply at 5.0 Å. This was due to the fact that the E_F was just below the E_c of the 5.0 Å case, and hence, any decrease in D would have “activated” the device. This also indicated that the threshold voltage could be tuned by controlling the doping level.

Lastly, a parallel plate actuator floating gate design^{21,22} to explore the concept of BG NR NEMS switch was explored, and an analysis on the device characteristics was carried out. An electrostatic doping of 0.25 eV was assumed, and the channel width and length of the device were taken to be 1.1 and 10.1 nm, respectively. The gate of the device was assumed to have an area about five times of that of the channel, and a 5-nm-thick silicon dioxide was placed between the mobile gate and the top layer of the BG NR. A schematic of the floating gate is depicted in Figs. 3(b) and 3(c) for the ON-state and OFF-state, respectively. The BG NR considered in this study had a Bernal stacking order and the pressure required to change D , as well as the total energy of the system, were extracted as shown in Fig. 3(a). The pressure plot shows that there are two stable states for the system, namely, at 3.2 and larger than 5.0 Å, where the pressure is close to zero. A perpendicularly applied pressure of 5.51 nN/nm² was required for the system to switch between the two different stable states. The perpendicular pressure and the electrostatic doping are important parameters to consider when applying the BG NR device as a sensor or as an electromechanical switch [cf. Figs. 1(a) and 1(b), respectively].

The NEMS switch was at ON-state initially (where the $D=0.31$ nm) at zero gate bias ($V_G=0$), and as V_G increased, F_E (the spring force) increased. When F_E became greater than the sum of the interlayer force between BG NRs (F_{GNR})

and F_S , the mobile electrode moved toward the fixed electrode, increasing D of BGNRs. An analytic equation relating V_G with the change in D (Δd) using the parallel plate actuator model is

$$V_G = \sqrt{\frac{2t_{\text{gap}}^2(F_{\text{GNR}} + \kappa\Delta d)}{A\varepsilon_{\text{gap}}}}, \quad (1)$$

with t_{gap} being the distance between the fixed and mobile electrodes, κ is the spring constant of the oxide hinges, and ε_{gap} is the dielectric constant of the air gap between the electrodes.

When $D=0.365$ nm for $V_G=5.6$ V in the current model, F_{GNR} was at its maximum [as shown in Fig. 3(a)], after which F_E would always be larger than the sum of F_{GNR} and F_S , and hence the fixed and mobile electrode came into contact, causing D to increase suddenly to beyond 0.50 nm, decreasing the current output. The gate bias where this occurs is defined as the threshold voltage (V_{th}) where the device switches from ON-state to OFF-state. Note that once the electrodes are in contact, they do not separate²³ until the V_G is 0 and when that happens, F_S , together with F_{GNR} , will cause D to decrease, leading to an abrupt increase in current, switching the device from OFF-state to ON-state. The current characteristic under different V_G for the proposed NEMS switch is plotted in Fig. 3(e) with the solid line showing the device being turned OFF at V_{th} , and the dashed line showing the current with the V_G being reversed. While further design modification is required to optimize the device performance, the BGNR NEMS switch shows great potential for application in memory devices.

In summary, the operating principle of BGNR devices was explored in this letter. It was found that the current characteristic of the device was intimately coupled to the interlayer distance D . As D decreased, the E_g of the channel material decreased and the current of the device increased as a result. Moreover, the perpendicular pressures on the device at different D were extracted, and to switch the device, a pressure of about 5.51 nN/nm² was required. These promising characteristics of BGNR devices led to the potential applications of NEMS sensor and switches, and hence, we introduced a prototype of a BGNR floating gate NEMS switch and presented its working principle and device performance. The device exhibited an $I_{\text{ON}}/I_{\text{OFF}}$ ratio to reach a magnitude of 3 orders under a low operation bias of 20 meV. Further device performance optimization could be done, for example, by increasing the channel length, adjusting the

Fermi level position via electrostatic doping and reducing the effective gap thickness.

This work is supported by A*STAR SERC Grant No. 0821010023 and National Research Foundation CRP “Graphene and related materials and devices.”

- ¹S. N. Cha, J. E. Jang, Y. Choi, G. A. J. Amaratunga, D.-J. Kang, D. G. Hasko, J. E. Jung, and J. M. Kim, *Appl. Phys. Lett.* **86**, 083105 (2005).
- ²Z. Chen, L. Tong, Z. Wu, and Z. Liu, *Appl. Phys. Lett.* **92**, 103116 (2008).
- ³H. J. Hwang and J. W. Kang, *Physica E* **27**, 163 (2005).
- ⁴S. Fujita, K. Nomura, K. Abe, and T. H. Lee, *IEEE Trans. Circuits Syst.* **54**, 2472 (2007).
- ⁵K. L. Ekinci, X. M. H. Huang, and M. L. Roukes, *Appl. Phys. Lett.* **84**, 4469 (2004).
- ⁶J. P. Hollingsworth and P. R. Bandaru, *Appl. Phys. Lett.* **87**, 233115 (2005).
- ⁷L. Maslov, *Nanotechnology* **17**, 2475 (2006).
- ⁸J. E. Jang, S. N. Cha, Y. J. Choi, D. J. Kang, T. P. Butler, D. G. Hasko, J. E. Jung, J. M. Kim, and G. A. J. Amaratunga, *Nat. Nanotechnol.* **3**, 26 (2008).
- ⁹K. S. Novoselov, A. K. Geim, S. V. Morozov, D. Jiang, Y. Zhang, S. V. Dubonos, I. V. Grigorieva, and A. A. Firsov, *Science* **306**, 666 (2004).
- ¹⁰C. Berger, Z. Song, X. Li, X. Wu, N. Brown, C. Naud, D. Mayou, T. Li, J. Hass, A. N. Marchenkov, E. H. Conrad, P. N. First, and W. A. de Heer, *Science* **312**, 1191 (2006).
- ¹¹X. Li, X. Wang, L. Zhang, S. Lee, and H. Dai, *Science* **319**, 1229 (2008).
- ¹²M. C. Lemme, T. J. Echtermeyer, M. Baus, and H. Kurz, *IEEE Electron Device Lett.* **28**, 282 (2007).
- ¹³Y.-W. Son, M. L. Cohen, and S. G. Louie, *Phys. Rev. Lett.* **97**, 216803 (2006).
- ¹⁴S. B. Trickey, F. Müller-Plathe, and G. H. F. Dierksen, *Phys. Rev. B* **45**, 4460 (1992).
- ¹⁵E. McCann, *Phys. Rev. B* **74**, 161403(R) (2006).
- ¹⁶J. Nilsson, A. H. C. Neto, F. Guinea, and N. M. R. Peres, *Phys. Rev. B* **76**, 165416 (2007).
- ¹⁷L. M. Zhang, Z. Q. Li, D. N. Basov, M. M. Fogler, Z. Hao, and M. C. Martin, *Phys. Rev. B* **78**, 235408 (2008).
- ¹⁸Z. Q. Li, E. A. Henriksen, Z. Jiang, Z. Hao, M. C. Martin, P. Kim, H. L. Stormer, and D. N. Basov, *Phys. Rev. Lett.* **102**, 037403 (2009).
- ¹⁹K.-T. Lam and G. Liang, *Appl. Phys. Lett.* **92**, 223106 (2008).
- ²⁰ATK Manual, “ATK version 2008.02,” ATOMISTIX A/S www.atomistix.com; M. Brandbyge, J.-L. Mozos, P. Ordejón, J. Taylor, and K. Stokbro, *Phys. Rev. B* **65**, 165401 (2002); J. M. Soler, E. Artacho, J. D. Gale, A. García, J. Junquera, P. Ordejón, and D. Sánchez-Portal, *J. Phys.: Condens. Matter* **14**, 2745 (2002); J. Taylor, H. Guo, and J. Wang, *Phys. Rev. B* **63**, 245407 (2001). The details of simulation parameters used are as follows: the local density approximation (LDA) exchange-correlation function with the double- ζ basis set was implemented and the effect of core electrons was described with the default pseudopotential parameters.
- ²¹B. Pruvost, H. Mizuta, and S. Oda, *IEEE Trans. Nanotechnol.* **6**, 218 (2007).
- ²²N. Abelé, R. Fritschi, K. Boucart, F. Casset, P. Ancy, and A. M. Ionescu, *Tech. Dig. - Int. Electron Devices Meet.* **2005**, 479.
- ²³M.-H. Bao, *Micro Mechanical Transducers: Pressure Sensors, Accelerometers and Gyroscopes* (Elsevier, Amsterdam, 2000), Chap. 4.